Synthesis of a δ-SnS Polymorph by Electrodeposition

Jeffrey R. S. Brownson, Cécile Georges, and Claude Lévy-Clément*

Laboratoire de Chimie Métallurgique des Terres Rares, CNRS, UPR 209, Bât. F, 2-8 rue Henri Dunant, 94320 Thiais, France

Received August 4, 2006. Revised Manuscript Received September 25, 2006

A new SnS polymorph (δ-SnS) has been obtained by cathodic electrodeposition on SnO_2:F glass electrodes from warm (50−90 °C) acidic solutions with tartaric acid. Characterizations of the as-deposited films by energy dispersive spectroscopy confirm a 1:1 Sn/S chemistry, X-ray diffraction shows that δ-SnS has a primitive orthorhombic symmetry, and UV/vis spectroscopy shows a direct optical band gap of 1.05 eV. The structure was converted to the α-SnS phase (reduced *a* and *c* lattice constants, direct optical transition of 1.2 eV) following argon annealing above 270 °C. Scanning electron microscopy images indicate pseudomorphic replacement of plate-like nanoparticles after annealing.

Introduction

Thin film materials are being studied to harvest light as a component in advanced photovoltaics.[1−3] The requirements of any new absorber materials are such that they are inexpensive, environmentally benign, and help to improve energy conversion efficiencies in solar cell devices.[2−5] Tin monosulfide (SnS) has great potential in all of these respects and, hence, is a material of interest in advanced photovoltaic devices.

SnS absorbs light within peak range for the standard AM 1.5 solar spectrum (1.1−1.4 eV) and has been found to have a high absorptivity coefficient ($\alpha > 10^4$ cm^{-1}).[4−6] Although β- and γ-SnS polymorphs have been reported,[7−9] α-SnS is the most frequently synthesized phase (also termed herzenbergite) and is a p-type semiconductor characterized by a direct optical transition of ∼1.3 eV.[3−5] For the electronic valence configuration in SnS, the sulfur atoms have been calculated to be more electronegative, drawing an electron pair (as [Ne]$3s^2 3p^6$) away from tin. The tin atoms consequently have an oxidation state of 2+ ([Kr]$4d^{10}5s^2 5p^0$).[10] In SnS, the additional nonbonding 5s electrons of the tin are found as lone pairs that strongly distort the lattice from a rocksalt structure common to tin monochalcogenides, to an orthorhombic layered structure found in α-SnS (see Table 1; PDF 73-1859).[10−12]

α-SnS has been investigated in the past as a material for solar cell[3−5] and battery[13] applications, but single-phase yields have only recently been reported. Consistent experimental results have been acquired from spray pyrolysis, chemical deposition, and mechanochemical synthetic methods.[3−5,13] Electrodeposition experiments have also been pursued as methods toward SnS thin film deposition; however, they have yielded a broad range of results, and only a few have yielded single phase tin monosulfide (α-SnS). Mishra et al.[14] proposed a room-temperature cathodic method in ethylene glycol but experienced poorly adherent films, anion contamination, amorphous materials, and widely ranging Sn/S ratios enriched in tin. Zainal et al.[15] attempted potentiostatic methods at room temperature in N_2-purged acidic solutions using $SnCl_2$ and $Na_2S_2O_3$ (∼1:1 molar ratio of Sn/S) and reported a mixture amorphous material, oxides, and tin metal. Ghazili et al.[16] attempted a similar potentiostatic method using $SnCl_2$ and $Na_2S_2O_3$ with ethylenediaminetetraacetic acid to some success, but the authors found an unusual mixture of a second crystalline phase by X-ray diffraction (XRD). Ichimura et al.[17] proposed a potentiostatic method in acidic aqueous solutions of $Sn(SO_4)_2$ and $Na_2S_2O_3$ but also found Sn/S ratios enriched in tin (suggesting metal co-

* To whom correspondence should be addressed. Tel.: +33 (0)1 49 78 12 01. Fax: +33 (0)1 49 78 12 03. E-mail: levy-clement@glvt-cnrs.fr.

(1) Hodes, G. In *Physical Eelectrochemistry: Principles, Methods, and Applications*; Monographs in electroanalytical chemistry and electrochemistry; Rubinstein, I., Ed.; Marcel Dekker, Inc.: New York, 1995; pp 515−553.
(2) Memming, R. *Electrochim. Acta* **1980**, *25*, 77.
(3) Nair, M. T. S.; Nair, P. K. *Semicond. Sci. Technol.* **1991**, *6*, 132.
(4) Koteeswara Reddy, N.; Ramakrishna Reddy, K. T. *Physica B* **2005**, *368*, 25.
(5) Koteeswara Reddy, N.; Ramakrishna Reddy, K. T. *Mater. Res. Bull.* **2006**, *41*, 414.
(6) Green, M. A. In *Solar Energy: The State of the Art;* ISES Position Papers; Gordon, J., Ed.; James and James, Ltd.: London, U.K., 2001; pp 291−355.
(7) von Schnering, H.-G.; Weidemeier, H. Z. *Kristallografiya* **1981**, *156*, 143.
(8) Nozaki, H.; Onoda, M.; Sekita, M.; Kosuda, K.; Wada, T. *J. Solid State Chem.* **2005**, *178*, 245.
(9) Ehm, L.; Knorr, K.; Dera, P.; Krimmel, A.; Bouvier, P.; Mezouar, M. *J. Phys.: Condens. Matter* **2004**, *16* (21), 3545.
(10) Lefebvre, I.; Szymanski, M. A.; Olivier-Fourcade, J.; Jumas, J. *Phys. Rev. B* **1998**, *58* (4), 1896.
(11) Walsh, A.; Watson, G. W. *J. Phys. Chem. B* **2005**, *109* (40), 18868.
(12) del Bucchia, S.; Jumas, J. C.; Maurin, M. *Acta Crystallogr.* **1981**, *37B*, 1903.
(13) Li, Y.; Tu, J. P.; Wu, H. M.; Yuan, Y. F.; Shi, D. Q. *Mater. Sci. Eng. B* **2006**, *128*, 75.
(14) Mishra, K.; Rajeshwar, K.; Weiss, A.; Murley, M.; Engelken, R. D.; Slayton, M.; McCloud, H. E. *J. Electrochem. Soc.* **1989**, *136*, 1915.
(15) Zainal, Z.; Hussein, M. Z.; Ghazili, A. *Sol. Energy Mater. Sol. Cells* **1996**, *40*, 347.
(16) Ghazali, A.; Zainal, Z.; Hussein, M. Z.; Kassim, A. *Sol. Energy Mater. Sol. Cells* **1998**, *55*, 237.
(17) Ichimura, M.; Takeuchi, K.; Ono, Y.; Arai, E. *Thin Solid Films* **2000**, *361*−362, 98.

10.1021/cm061841t CCC: $33.50
Published on Web 12/19/2006

Table 1. Calculated Lattice Constants of SnS Structures for pH 2.5 Tartaric Acid Solutions with Respect to Deposition Temperature[a]

sample conditions	*a*	*b*	*c*	*c*/*b*	*a*/*b*
α-SnS (PDF no. 73-1859)	11.180	3.982	4.329	1.09	2.81
pH 2.5/0.2 M/70 °C, as-deposited	11.380	4.029	4.837	1.20	2.82
pH 2.5/0.2 M/70 °C, annealed	11.172	3.994	4.311	1.08	2.80

[a] Each sample fit had an average difference $2\theta_{exptl} - 2\theta_{calcd} < 0.05$.

deposition) and poorly crystallized films. Sato et al.[18] attempted a pulsed potentiostatic method that yielded Sn/S ratios near 0.5, indicating SnS_2 precipitation or sulfur contamination in the films.

There are a few successful examples of SnS electrodeposition. Subramanian et al.[19] do not state their electrodeposition conditions, but appear to have deposited α-SnS using 5 mM $SnCl_2$ and 2.5 mM $Na_2S_2O_3$ (1:1 molar ratio of Sn/S) in pH 1.5 solution (one-quarter the concentration of $Na_2S_2O_3$ from Zainal et al.). Cheng et al.[20] also reported α-SnS using a galvanostatic method at pH 2.7 with <20 mM $Sn(SO_4)_2$ and <100 mM $Na_2S_2O_3$ (1:10 molar ratio of Sn/S, excluding sulfate) on Pt electrodes. And recently Gordillo et al.[21] also reported α-SnS using a galvanostatic method with 50 mM $SnCl_2$, 150 mM $Na_2S_2O_3$ (1:6 molar ratio of Sn/S), and organic buffer solutions of tartrate, citrate, and acetate and their respective conjugate acids.

We have found a facile method of SnS film electrodeposition by simplifying the method of Gordillo et al., which requires only an organic acid additive with tin and sulfur precursors in aqueous solution. The addition of tartaric acid is required and aids thin film adhesion and phase stability but also facilitates a distinct new polymorph of SnS to be deposited.

Experimental Section

Anhydrous tin(II) chloride ($SnCl_2$, Aldrich), sodium thiosulfate ($Na_2S_2O_3$, Aldrich), and L-(+)-tartaric acid ($C_4H_6O_6$, VWR) were used for the tin, sulfur, and organic additives in solution, respectively. Starting solutions of 0.1 M HCl, created from freshly collected ultrapure water (18.2 MΩ·cm) and purged continuously with nitrogen, were used to minimize Sn^{2+} oxidation. At room temperature, the organic acid was dissolved into the HCl solution with stirring (0.2 M tartaric acid in 100 mL of final solution). In each system, $SnCl_2$ and $Na_2S_2O_3$ were added to yield 50 mM and 150 mM concentrations, respectively (1:6 molar ratio of Sn/S). $SnCl_2$ was solvated in 10 mL of acetone prior to mixing with the acidic aqueous solution to fully dissolve the precursor.[3] When mixed with 90 mL of the HCl and tartaric acid, a clear solution resulted. Finally, $Na_2S_2O_3$ was added, the pH was adjusted to 2.5 with NaOH, and the solution was transferred into a three-necked flask flushed with N_2(g). A sealed salt bridge of the mother solution was mounted between the reaction vessel and a saturated KCl solution holding the reference electrode.

Cyclic voltammetry (CV) and electrodeposition were performed using an Autolab PGSTAT100 potentiostat/galvanostat and GPES software (Eco Chemie B.V., NL). A three-electrode electrochemical cell was employed in all electrodeposition and CV experiments. A standard calomel electrode (SCE), a coiled Pt wire, and transparent conductive oxide (TCO)-coated glass slides (SnO_2:F) having a sheet resistance of 10 Ω/□ were used as the reference, counter, and working electrodes, respectively. TCO substrates were cleaned with mild detergent (glycerol free) and ultrapure water, and a geometric surface of 1 cm^2 was masked off prior to electrodeposition.

CV characterization was performed at 70 °C for the separate precursor components ($SnCl_2$, $Na_2S_2O_3$) and the complete solution. Starting solutions contained 0.2 M tartaric acid/0.1 M HCl/10 vol % acetone. A set of organic control voltammograms were collected for the starting solutions ($[C_4H_6O_6] = 0.2$ M and $[HCl] = 0.1$ M) with and without acetone. All scans were carried out from solution rest potential (near zero), with a cathodic sweep to −1 V versus SCE and then an anodic sweep to +0.4 V. Scans were performed at a rate of 150 mV/s.

Cathodic electrochemical depositions were performed at 70 °C under galvanostatic conditions. "As-deposited" films were cleaned of residual chloride and tartrate salts as well as particulate elemental sulfur using three successive washes of acetone, propanol, and water before being dried in air at room temperature and being characterized by scanning electron microscopy (SEM; Leo 1530, 3 kV accelerating voltage), electron dispersive spectroscopy (EDS; PGT intrinsic Ge detector), thermal gravimetric analysis (TGA), XRD (Cu $K\alpha_1$, $\lambda = 1.540\,56$ Å), and UV/vis spectroscopy (Hitachi Digilab U-4100 with integrating sphere). In order to avoid the undesirable tin emission contributed by the SnO_2:F substrate for EDS data collection, powders were prepared by scraping the films onto carbon tape. The powders were analyzed in 10 separate locations each, with an accelerating voltage of 15 kV and an acquisition time of 100 s. EDS data were corrected for absorption effects by phi-rho-Z integration. TGA and differential thermogravimetry (dTG) were also performed on a powder collected from an as-deposited film using an Ar gas atmosphere.

Analysis of XRD peaks was performed with a least-squares linear regression software (XRF3).[22] Given a series of selected peaks, a symmetry group, and a likely initial set of lattice parameters, the program converged on a best fit of lattice parameters for the material in question. Peaks belonging to the SnO_2 substrate were excluded from the set of data for fitting.

UV/vis spectra were collected for each film using transmission and reflectivity measurements, and absorption spectra were calculated from the two measurements. Transmission data were corrected for the contribution by the TCO substrate prior to absorption calculations. Following the initial tests, as-deposited films were annealed at 350 °C for 30 min under an Ar atmosphere and characterized again. To establish a temperature of phase transition of the as-deposited films to α-SnS, independent annealing tests were performed on as-deposited films from 130 °C to 330 °C (20 min each, under an Ar atmosphere).

Results and Discussion

Solution Behavior. Under acidic conditions or UV illumination, thiosulfate is unstable and undergoes disproportionation to yield a suspension of colloidal sulfur and

(18) Sato, N.; Ichimura, M.; Arai, E.; Yamazaki, Y. *Sol. Energy Mater. Sol. Cells* **2005**, *85*, 153.
(19) Subramanian, B.; Sanjeeviraja, C.; Jayachandran, M. *Mater. Chem. Phys.* **2001**, *71*, 40.
(20) Cheng, S.; Chen, Y.; Huang, C.; Chen, G. *Thin Solid Films* **2006**, *500*, 96.
(21) Gordillo, G.; Téllez, A.; Romero, E.; Quiñónez, C.; Rodriguez, O. In *20th European Photovoltaic Solar Energy Conference Proceedings*, Barcelona, Spain, June 6−10, 2005; Palz, W., Ossenbrink, H., Helm P., Eds.; pp 326−329.
(22) Godart, C.; Alleno, E. LCMTR internal software program, 1995.

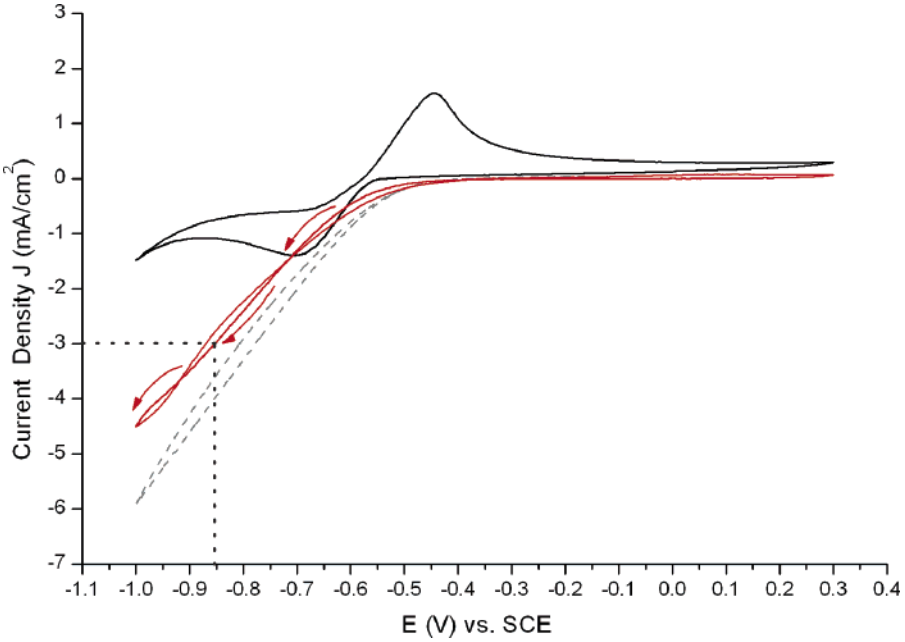

Figure 1. Cyclic voltammograms (150 mV/s) at 70 °C, pH 2.5. Scans for tin chloride (solid black), thiosulfate (dashed gray), and the full precursor system (solid red). Initial deposition conditions: −3 mA/cm^2 and −0.86 V vs SCE indicated with short dashed lines.

dissolved bisulfite (eq 1).[1,23,24] Room-temperature disproportionation at the initial pH of 1.4 occurs within minutes. When the Sn and S precursors are present with the tartaric acid additive, the suspending solution turns a transparent bright yellow hue (distinct from the colloidal sulfur particles). An odor of $H_2S(g)$ is also present with this yellow system. In the absence of tartaric acid, neither a yellow hue nor a hydrogen sulfide odor is present, and the colloidal sulfur appears as a whitish cloudy suspension. Additionally, the yellow hue is absent in solutions with only dissolved Sn^{2+} and tartaric acid.

$$S_2O_3^{2-} + H^+ \rightarrow S^0(s) + HSO_3^- \quad (1)$$

CV. In Figure 1 we illustrate the CV responses of the TCO films in solution/suspension. The onset of a cathodic current at the electrode surface within the tin solution ($[Sn^{2+}] = 5$ mM) occurs at approximately −0.56 V vs SCE. In contrast, the onset of the cathodic current for the sulfur/bisulfite suspension ($[S_2O_3^{2-}] = 150$ mM) appears at a slightly lower voltage near −0.45 V vs SCE. The cyclic voltammogram of the system having the full tin/sulfur chemistry (full precursor suspension) displays a gradual cathodic current onset roughly intermediate to that of the two components. However, as indicated in Figure 1, for a selected current density of deposition of −3 mA/cm^2 the measured initial voltage was significantly higher, at −0.86 V. This observed potential is very similar to the sulfur species CV data at the same current density. Hence, for the higher potentials measured during galvanic electrodeposition, sulfur species reduction may be the dominant current contributor in SnS electrodeposition with a tartaric acid additive. Equation 2 presents the suggested general reaction for SnS formation.

$$Sn^{2+} + S^0 + 2e^- \rightarrow SnS \quad (2)$$

The CV spectra of tartaric acid solutions (not shown) were found to have minimal current contributions in the potential range studied, effectively removing tartaric acid reduction as a major contributing factor in the system. The curves were very similar with and without acetone, suggesting that acetone does not strongly affect the electrochemistry of the system either. These data indicate that the active species in the electrodeposition experiments appear to be related solely to the tin and sulfur species.

Film Characterization. *1. As Deposited Films.* The SEM image in Figure 2a show that films deposited galvanostatically at $J = -3$ mA/cm^2, for 1500 s, and a charge density of $\sigma = 4.5$ C/cm^2 at 70 °C yielded anisotropic platelike forms with multiple secondary nucleation plates growing orthogonal to a central plate. Resulting galvanostatic as-deposited films were matte black when dried. Film thickness was estimated at 600−700 nm by SEM cross-section analysis.

The XRD spectra of the as-deposited samples are shown in Figure 3 (red curve). Beside the Bragg diffraction peaks related to the SnO_2 of the conductive glass, a set of well-defined peaks are observed. All the peaks could be attributed to the deposited film and indexed in an orthorhombic structure similar to α-SnS, yet different. The peaks were slightly shifted compared to the *hkl* peaks reported in the α-SnS JCPDS file calculated from the results of del Bucchia et al.[12] ($a = 11.180$ Å, $b = 3.982$ Å, $c = 4.329$ Å).[25] The least-squares calculated fits of the lattice constants and the resulting lattice ratios are presented in Table 1. Analyses of the data confirmed that the as-deposited structure was also a primitive orthorhombic structure, but with larger ***a*** and ***c*** lattice constants (***a***= 11.380 Å ***b***= 4.029 Å ***c***= 4.837 Å). The new structure did not match SnS_2 or Sn metal diffraction

(23) Pourbaix, M. *Atlas of Electrochemical Equilibria in Aqueous Solutions*, 2nd ed.; National Assoc. Corrosion Engineers: Houston, TX, 1974.
(24) Marandi, M.; Taghavinia, N.; Irajizad, A.; Mahdavi, S. M. *Nanotechnology* **2005**, *16*, 334.
(25) Powder Diffraction File 73-1859, PDF-2 Database Sets; International Center for Diffraction Data: Newton Square, PA, 1993.

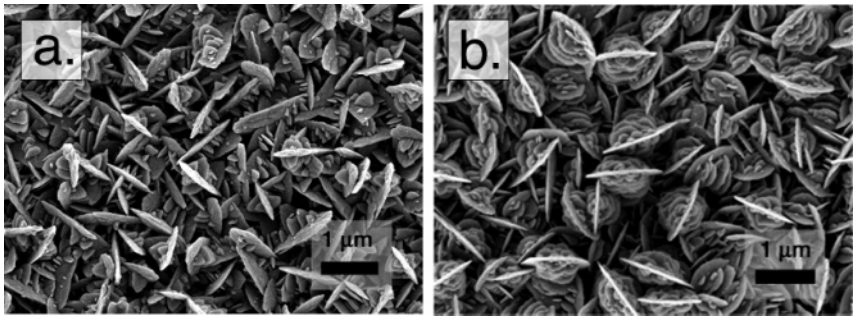

Figure 2. SEM images of two tartaric acid-modified SnS films. (a) As-deposited film. (b) Annealed film (350 °C under argon).

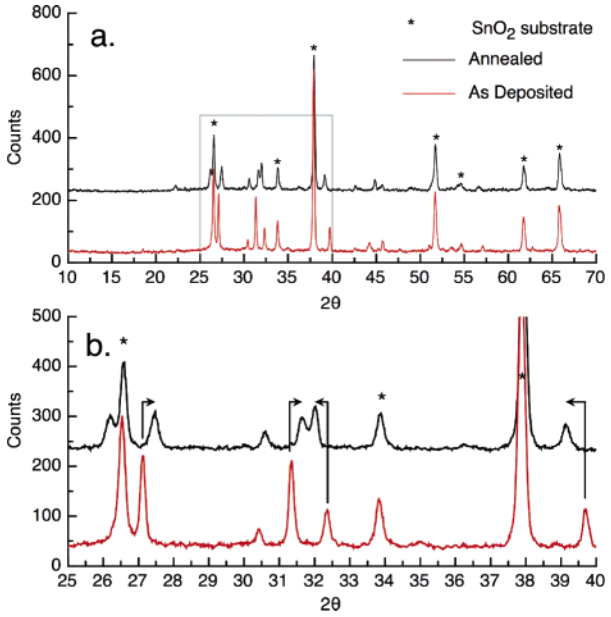

Figure 3. (a) XRD patterns of tartaric acid-modified SnS films before and after annealing (red and black, respectively). (b) Expanded region from 25 to 40° 2θ. Arrows indicate shifts in crystal structure from δ-SnS to α-SnS.

patterns. Powders scraped from as-deposited films that were analyzed by EDS had a mean Sn/S ratio of 0.97 (±0.04; 95% confidence interval), confirming a tin monosulfide phase.

Structural distortion appears to be dependent on the presence of tartaric acid in the precursor suspending solution. We have reviewed the literature for SnS polymorphs and found that the β-SnS and γ-SnS phase has been reported previously.[7−9] However, these are a high temperature and a high-pressure phase having base-centered orthorhombic and monoclinic symmetries, respectively. The XRD data were non-convergent with either phase when analyzed. Hence, we propose that this structure be termed δ-SnS.

2. Annealed Films. Films were annealed at 350 °C to improve disorder in the film crystallinity but were found to convert the distorted δ-SnS phase into the α-SnS phase. Annealed films were also black but gained a slightly glossy appearance. Annealing did not alter the gross morphology of the films; however, slight variation occurred between samples with respect to the degree of secondary nucleation and morphology of the central plate from triangular to rounded shape, seen in the SEM image of Figure 2b.

The crystalline phase present in the annealed films (***a***= 11.172 Å ***b***= 3.994 Å ***c***= 4.311 Å) was found to agree

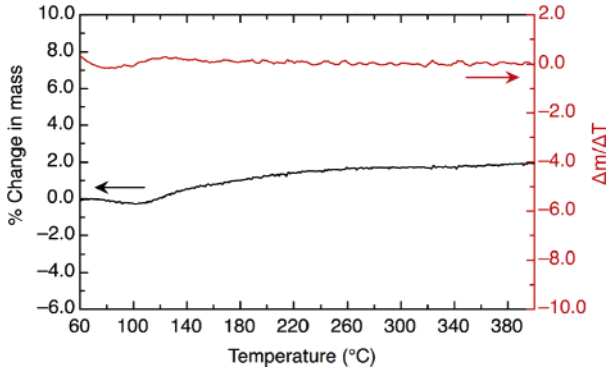

Figure 4. TGA of tin monosulfide material with TG (black) and dTG (red) indicated.

closely with the α-SnS presented as PDF 73-1859 in the Table 1 (a = 11.180 Å, b = 3.982 Å, c = 4.329 Å).[25] In Figure 3, we show a representative example of a diffraction pattern for films deposited at 70 °C, and the subsequently altered patterns for those films with annealing at 350 °C. For EDS analysis, the mean Sn/S ratio with annealing was 0.99 (±0.02; 95% confidence interval). These data suggest both the as-deposited thin films and the annealed films are tin monosulfide.

In Figure 4, we show TGA data supporting the interpretation of a crystal structure transition without change in mass. The mass changes during TGA were measured to be less than 2% from 60 °C to 400 °C for as-deposited powders. Careful examination by calculated dTG revealed that the slight increase was related to an incremental linear drift in the baseline. Separate annealing experiments between 130 °C and 330 °C confirmed a phase transition of δ-SnS → α-SnS between 200 °C and 270 °C, with a mixture of phases observed by XRD at 240 °C. As demonstrated in Figure 4, between 200 °C and 270 °C, the phase transition was not accompanied by a significant mass change. If a contaminating organic component were present, a definite dTG mass loss would have been expected, which could then be attributed to the organic decomposition. This confirms that the δ-SnS is not a compound distorted by guest organics.

As the two structures are very similar, we can gain insight by considering the α-SnS structure in Figure 5 (unit cell delineated) as a basis for the distorted structure of the as-deposited film. Within the unit cell, two tin atoms and their bonding configurations are presented; short, strong bonds are shown by short dashed lines, while longer weak bonds are shown by doted lines (and not represented outside the unit cells). Arrows indicate the presence of lone-pair

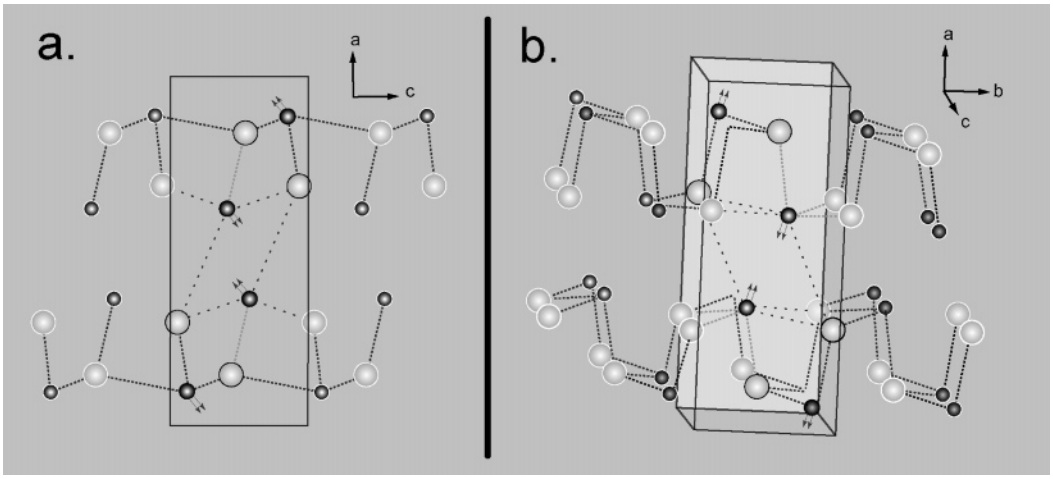

Figure 5. Structure of α-SnS (adapted from refs 7 and 9). (a) Cross section of the *b* zone axis. (b) 3-D unit cell projection of the *c* zone axis (tilted). Dark and light spheres represent tin and sulfur atoms, respectively (unit cell atoms: outlined in black).

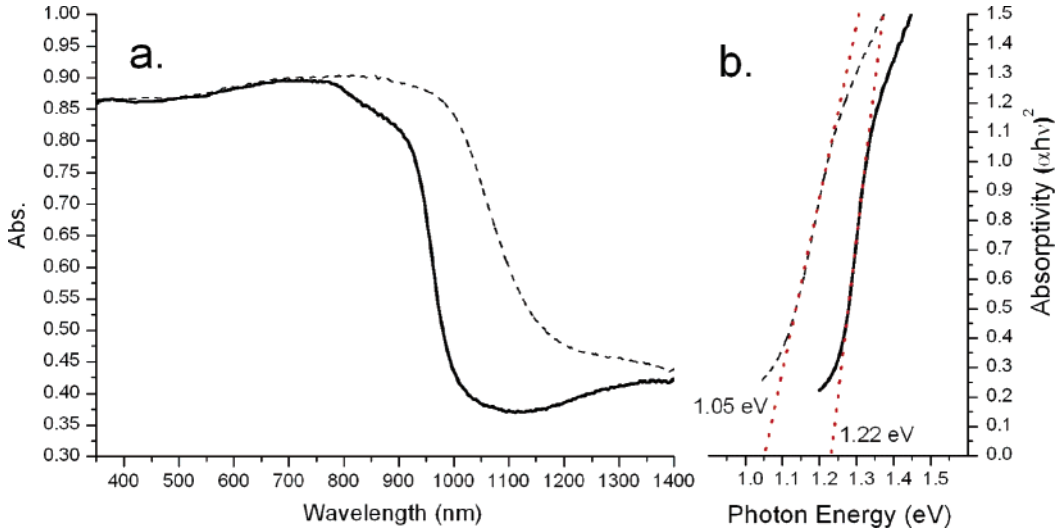

Figure 6. (a) UV/vis absorption spectra of SnS films as-deposited (δ-SnS; dashed line) and after annealing (α-SnS; solid line). (b) Absorptivity plot assuming a direct allowed transition for the same spectra.

electrons. One finds that each tin atom is sixfold coordinated with surrounding sulfur atoms. This coordination can be viewed as a highly distorted octahedron composed of three short Sn−S bonds (two 2.66 Å/one 2.63 Å) and three weak longer Sn−S bonds (two 3.29 Å/one 3.39 Å).[10] As seen in Figure 5, the short bonds are divided into two distinct layers in the unit cell, while the longest of the weak bonds is stretched across the interlayer gap. The lone pair of electrons is then concentrated inside the tripod of weak bonds. Assuming that structural distortion in the δ-SnS phase occurs in the as-deposited films without breaking covalent bonding, deformation is expected to occur along the zone axes orthogonal to these stable layers (the *a* zone axis). But it is unusual to find additional lattice expansion along the *c* zone axis, with virtually no change in the *b* lattice constants between the δ-SnS and the α-SnS phases (see Table 1). However, this structure is expected to be strongly affected by the lone-pair electrons protruding from each tin atom.[10−12] A potential hypothesis for the second lattice expansion is a glide-plane translation between the layers along the *c* zone axis, in addition to the interlayer expansion. Perhaps interlayer expansion is accompanied by preferential shear along the *c* zone axis.

UV/Vis Spectroscopy. In Figure 6a we show the corrected absorption spectra for the as-deposited and annealed films. The absorption onset shifts from longer to shorter wavelengths with annealing under argon, and both films showed some additional absorption at longer wavelengths. We attribute this contribution to light scattering effects by the platelike particles. In Figure 6b we show that the two materials have two distinct optical absorption transitions. The as-deposited (δ-SnS) thin film displayed a direct optical transition at 1.05 eV. After the films were annealed at 350 °C, the resulting thin film (α-SnS) displayed increased band gap absorption energy of 1.2 eV, again obeying a direct optical transition, consistent with α-SnS.[3−5] Preliminary electrochemical experiments in ferri-/ferrocyanate ($[Fe(CN)_6]^{3-}/[Fe(CN)_6]^{4-}$) solutions show that the δ-SnS thin films are photoactive, displaying p-type behavior. The present optical data are intriguing, as the energy values reported in the literature for SnS have varied widely depending on synthesis conditions (1.0−1.4 eV).[3,4,14−21] This range may

be explained by possible misinterpretation of δ-SnS as the alternate polymorph, α-SnS, which has many similarities (1:1 Sn/S ratio, p-type, direct transition and a similar XRD pattern), or the spread could be due to a mixture of both phases formed during synthesis. To our knowledge, this is the first time the δ-SnS phase has been isolated from the α-SnS, and the distinction in structure and optical band gaps between the two should aid in future SnS characterization.

Conclusions

We have presented a novel method for the electrodeposition of a new phase of tin monosulfide thin films (δ-SnS) in warm acidic aqueous solutions purged with nitrogen, with $SnCl_2$ and $Na_2S_2O_3$ precursors and a tartaric acid additive. Tartaric acid contributes to the formation of a yellow suspending solution with a hydrogen sulfide odor after thiosulfate disproportionation. Tartaric acid also aids in film uniformity and adherence. CV results suggest that sulfur species reduction may be the dominant current contributor in δ-SnS formation with a tartaric acid additive. The as-deposited δ-SnS phase appeared to have a significantly distorted structure with expanded *a* and *c* lattice constants compared to α-SnS, and a smaller direct optical band gap energy of 1.05 eV. The distorted structure was readily converted to α-SnS with annealing of the film under argon, yielding a thin film with a direct optical band gap of 1.2 eV, similar to that of recent α-SnS studies. Annealing did not change the morphology of the films despite the shift in crystal structure, indicating pseudomorphic replacement of δ-SnS with α-SnS. EDS data confirmed a 1:1 Sn/S stoichiometric ratio in as-deposited and annealed films, and TGA data indicated no significant mass change over a wide range of thermal conditions; however, XRD data indicated a distinct phase transition between 200 and 270 °C.

Acknowledgment. The authors sincerely thank Benjamin Villeroy at the CNRS Laboratoire de Chimie Métallurgique des Terres Rares in Thiais, France, for his assistance with the TGA experiments. We also thank IMRA-Europe for partial financial aid and for positive discussions regarding the research.

CM061841T